Efficient 2D and 3D Facade Segmentation using Auto-Context

Raghudeep Gadde*, Varun Jampani*, Renaud Marlet, and Peter V. Gehler

Abstract—This paper introduces a fast and efficient segmentation technique for 2D images and 3D point clouds of building facades. Facades of buildings are highly structured and consequently most methods that have been proposed for this problem aim to make use of this strong prior information. Contrary to most prior work, we are describing a system that is almost domain independent and consists of standard segmentation methods. We train a sequence of boosted decision trees using auto-context features. This is learned using stacked generalization. We find that this technique performs better, or comparable with all previous published methods and present empirical results on *all* available 2D and 3D facade benchmark datasets. The proposed method is simple to implement, easy to extend, and very efficient at test-time inference.

Index Terms— Auto-Context, Facade Segmentation, Semantic Segmentation, Stacked Generalization.

◆

1 INTRODUCTION

IN this paper, we consider the problem of segmenting building facades in an image, resp. a point cloud, into different semantic classes. An example image from a common benchmark dataset for this problem is shown in Fig. 1 along with a manual annotation. Being able to segment facades is a core component of several real world applications in urban modeling, such as thermal performance evaluation and shadow casting on windows. As evident from the example in Fig. 1, images of buildings exhibit a strong structural organization due to architectural design choices and construction constraints. For example, windows are usually not placed randomly, but on the same height; a door can only be found on the street-level, etc.

This problem is also an interesting test-bed for general-purpose segmentation methods that also allow strong architectural prior. As a result, it appears reasonable to assume that methods which incorporate such high-level knowledge will perform well in doing automatic facade segmentation. Following this, existing facade segmentation methods use complex models and inference technique to incorporate high-level architectural knowledge for better pixel-level segmentation. Some examples are Conditional Random Field (CRF) models that use higher-order potential functions [1, 2]. Another route are grammar-based models that include generative rules [3, 4, 5] and try to infer the choice of production rules at parse time from the image evidence.

Contrary to the philosophy of existing methods, we largely ignore domain-specific knowledge. We describe a generic segmentation method that is easy to implement, has fast test-time inference, and is easily adaptable to new datasets. Our key observation is that very good segmentation results can be achieved by pixel classifications methods that use basic image features in conjunction with auto-context features [6]. In this work, we develop a simple and generic auto-context-based framework for facade segmentation. The system is a sequence of boosted decision tree classifiers,

that are stacked using auto-context [6] features and learned using stacked generalization [7]. We stack three pixel classifiers using auto-context features for images and two classifiers for 3D point clouds. Fig. 1 shows an example segmentation result for various classification stages of our method. As can be seen in the visual result of Fig. 1, the segmentation result is successively refined by the auto-context classifiers, from their respective previous stage result. Using pixel-level classifiers along with generic image features has the advantage of being versatile and fast compared to existing complex methods. The entire pipeline consists of established components and we consider it to be a baseline method for this task. Surprisingly, our auto-context based method, despite being simple and generic, consistently performs better or on par with existing complex methods on all the available diverse facade benchmark datasets in both 2D and 3D. Moreover, the presented approach has favourable runtime in comparison to existing approaches for facade segmentation. Therefore, this approach defines a new state-of-the-art method in terms of empirical performance. It is important to note that by proclaiming so, we are not invalidating the use of existing methods, that make of domain-knowledge, for facade segmentation. Experiments suggest that more domain-specific models would benefit from better unary predictions from our approach. Moreover our findings also suggest that previous methods need to be carefully re-evaluated in terms of a relative improvement compared to a method like the proposed one.

A pixel or point-wise facade classification might not be a desired output for some applications. For instance, high level structural information is needed to construct Building Information Models (BIMs). We show how the pixel predictions we obtain can be used in a inverse procedural modeling system [4] that parses facade images. These rules are of interest in different applications and we show that an improved pixel-wise predictions directly translates into a better facade parsing result.

This paper is organized as follows. Related work is discussed in Section 2, followed by a detailed description of the auto-context segmentation setup in Section 3. Section 4 contains the experimental results and we conclude in Section 5.

- *Raghudeep Gadde and Renaud Marlet are with Université Paris-Est, LIGM (UMR 8049), CNRS, ENPC, ESIEE Paris, UPEM, France.*
- *Varun Jampani is with MPI-IS, Germany.*
- *Peter Gehler is with BCCN, University of Tubingen and MPI-IS, Germany.*
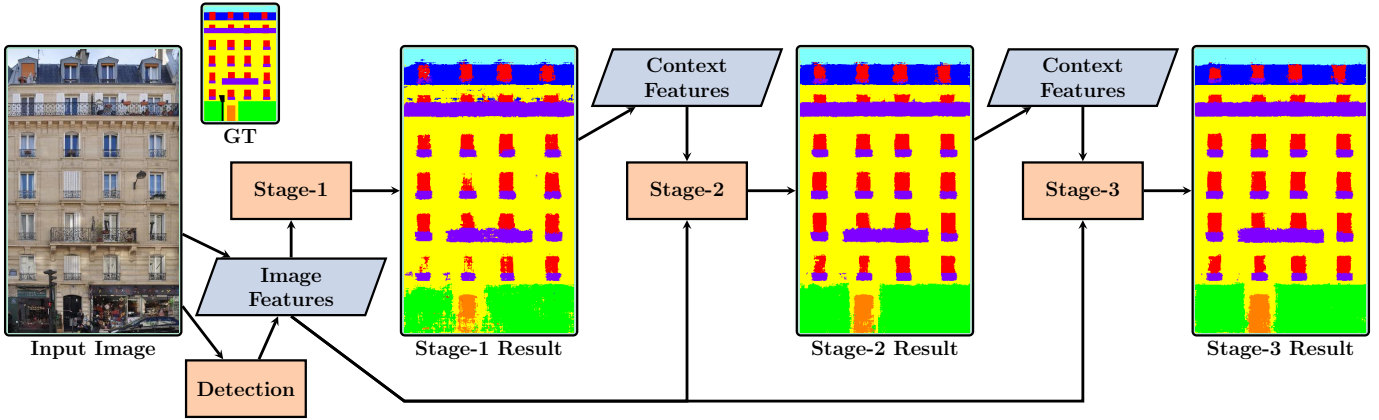- *The first two authors have contributed equally to this work.*

Fig. 1. Schematic of different components in our facade segmentation pipeline with a sample facade from ECP dataset [8]. 'Image' and 'Context' features correspond to features extracted on input image and previous-stage segmentation result respectively. 'Stage-n' refers to the nth stage auto-context classifier. The segmentation result is successively refined by the auto-context classifiers from their respective previous stage result.

2 RELATED WORK

Facade segmentation approaches can be broadly classified into two categories: *bottom-up methods* [9, 2, 1, 10] that use pixel-level classifiers in combination with CRF models and *top-down methods* [4, 3, 5, 11, 12] that use shape grammars or a user defined shape prior. The shape grammar methods seek to parse a facade in terms of a set of production rules and element attributes, thus segmenting the facade into semantic regions. The central idea is to represent the facade using a parse tree and search for the grammar derivation that best matches a pixel-level classification of an image. The high structural organization of facades due to architectural design choices make such a generative approach a natural model candidate. However it is not easily amendable to efficient inference, which often leads to inefficient and sub-optimal segmentation results. Furthermore, due to the strong prior that a grammar imposes, they are not necessarily pixel-wise accurate. As a consequence, the state-of-the-art methods in terms of pixel accuracy are dominated by the bottom-up methods, although they do not provide structured information as in a parse tree.

In [9, 13], a three-layered system is proposed. A first layer uses a recursive neural network to obtain pixel label probabilities, which are fed into a grid CRF model in a second layer along with object detections. The third layer enforces weak architectural principles in facades as post-processing. This setup combines high-level and low-level information into a single prediction. The runtime of this system is mentioned in [10] to be about 2 minutes for an image of size 500 by 300. Other approaches [1, 2] incorporate architectural knowledge in a single CRF framework using higher-order potential functions. The method of [1] proposes a hierarchical CRF framework to encode inter-class location information in facades. The work of [2] uses long-range pairwise and ternary potentials to encode the repetitive nature of various class regions. Both methods require specific inference techniques that result in non-negligible runtimes. The approach of [10] is to use a sequence of dynamic programming runs that search for optimal placement of window and balcony rows, door location and others. Every single step is very fast and the overall system is mostly global optimal. The downside is that the sequence and type of classifications needs to match facade architecture type. [12] employ a user-defined shape prior (an adjacency pattern) for parsing rectified facade images and formulates parsing as a MAP-MRF problem over a pixel grid.

Recently, techniques have been introduced for facade understanding and modeling in 3D [14, 15]. The 3D point cloud or meshes that these methods operate on are constructed using 2D images captured from multiple viewpoints. A standard way to label a 3D mesh or a point cloud, is to label all the overlapping images used for reconstructing the 3D model and then fuse the 2D predictions to obtain a consistently labeled 3D model [16, 17]. The work of [14] proposed a fast technique to segment 3D facade meshes by exploiting the geometry of the reconstructed 3D model. To label a mesh face, their approach selects a single 2D image (from the set of images used for reconstruction) that best captures the semantics. The speed of this technique comes at the cost of performance. The method of [15] implements a three-stage approach to label point clouds of facades directly in 3D. First, features on 3D points are computed and are classified into various semantic classes. Next, facades belonging to different buildings are separated based on previously obtained semantics. Finally, weak architectural rules are applied to enforce structural priors, leading to marginal improvements in performance (0.78% IoU) compared to the inital classifier predictions.

All the discussed methods build on top of semantic label probabilities which are obtained using pixel/point classifiers. It is only after those have been obtained that architectural constraints are taken into account. In the system we describe in this paper, 2D or 3D segmentations are obtained only using image or point cloud auto-context features without resorting to any domain specific architectural constraints. As a result, several above mentioned domain-specific approaches would benefit from using the segmentation label probabilities obtained with our proposed domain-independent approach.

The closest to our work are [18] and [19], which also proposed auto-context based methods for facade segmentation. [18] incorporated auto-context features in random decision forests where the classification results from top-layers of trees are used to compute auto-context features and are then used in training the lower layers of the trees in the forest. More recently, [19] proposed to use the local Taylor coefficients computed from the posterior at different scales as auto-context. Although [18] and [19] are conceptually similar, the method we propose uses different low-level features, different auto-context features and different learning techniques achieving better performance on benchmark datasets.

3 AUTO-CONTEXT SEGMENTATION

We propose an architecture that combines standard segmentation methods into a single framework. Boosted decision trees are stacked with the use of auto-context [6] features from the second layer onward. This system is then trained using stacked generalization [7]. We will describe the ingredients in the following, starting with the segmentation algorithm (Sec. 3.1), the feature representation for images (Sec. 3.2) and for point-clouds (Sec. 3.3), auto-context features (Sec. 3.4), and the training procedure (Sec. 3.5).

Given a point cloud or an image I, the task of semantic segmentation is to classify every point or pixel i into one of C classes $c_i \in \{1, \ldots, C\}$. During training, we have access to a set of N class-annotated images each with a variable number of points/pixels: $(I_i^j, c_i^j), j = 1, \ldots, N$. We will comment on the loss function in the experimental section and for now treat the problem as one that decomposes over the set of pixels. Two different feature sets are distinguished, data-dependent features $f_i \in \mathbb{R}^{D_f}$ that are derived from the spatial and color observations in a point cloud or image, and auto-context features $a_i \in \mathbb{R}^{D_a}$ based on the prediction results from previous stages.

3.1 Model Architecture

Our system consists of a sequence of classifiers as suggested in [6]. A schematic overview of the pipeline is depicted in Fig. 1. At every stage t, the classifier has access to the image and to predictions of all earlier stages. Formally, at stage $t > 1$ and at each pixel i, a classifier F^t maps image (I) and auto-context features (a_i) to a probability distribution P^t of the pixel class assignments

$$F^t\left(f_i(I), a_i(P^{t-1})\right) \mapsto P^t(c_i|I), \forall i. \qquad (1)$$

For pixel classifier F^t, we use boosted decision trees that store conditional distributions at their leaf nodes. In general, the output of F^t need not be a distribution. The first stage $t = 1$ depends only on the features $F^1(f_i(I))$ derived directly from the image. The setting is identical for point clouds.

This architecture is a conceptually easy and efficient way to use contextual information in pixel-level classification. Classifiers of later stages can correct errors that earlier stages make. An example sequence of predictions can be seen in Fig. 1. For example, an auto-context feature can encode the density of a predicted class around a pixel. The classifier can learn that certain classes only appear in clusters which then allows to remove spurious predictions. This has a similar smoothing effect as some pairwise CRF models have, but with the benefit of a much faster inference.

3.2 Image Features

As image features, we computed 17 TextonBoost filter responses [20], location information, RGB color information, dense Histogram of Oriented Gradients [21], Local Binary Pattern features [22], and all filter averages over image rows and columns at each pixel. These are computed using the DARWIN [23] toolbox.

In addition to the above generic segmentation features, we include detection scores for some specific objects. Following [9, 24, 25], we use detectors for windows as well as doors. Whereas [9, 24] fused the detection scores into the output of the pixel classifiers, we turned the detection scores into image features at every single pixel. We use the integral channel features detector from [26] for which a toolbox is available [27]. For a
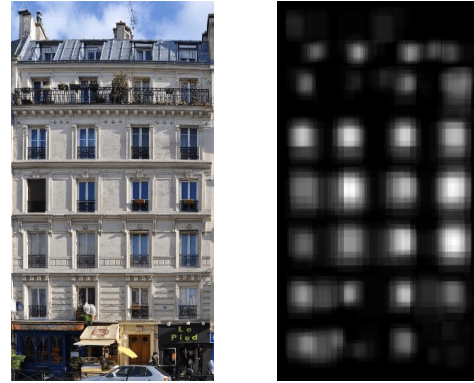

(a) Facade   (b) Detection

Fig. 2. (a) A facade and (b) its window detection scores. Bright and dark regions correspond to high and low detection scores respectively.

given image, the detector outputs a number of bounding boxes along with a corresponding score for each bounding box. We sum up the scores to get a single detection score at each pixel. Object detection parameters are automatically estimated using the training data to get a good recall. Fig. 2 shows an example window detection output for a sample facade image. The detection feature is of course a problem dependent one and based on the prior knowledge about the special classes: door and windows. However it is still a generic feature in the sense that the prior information is extremely weak and a generic detection system has been used to obtain it. Moreover, door and window classes are common to any architecture of facades. In the end, 761 low-level image features coupled with 2 door and window detection features make a total of 763 feature values at each pixel.

3.3 Point Cloud Features

We use the same set of features as [15] to describe a point cloud. The features inlude the mean RGB color values, their corresponding LAB values, the estimated normal at the 3D point, the spin image descriptor [28], the height of a point above an estimated groud plane, the depth of the point from an estimated facade plane and the inverse height of the point which is the distance from the uppermost point of the facade in the direction of the gravity vector. The combination of all these features form a 132-dimensional vector for every point.

3.4 Auto-context Features

In addition to the image features, the classifiers from stage $t > 1$ can condition on statistics computed from previous predictions. We include the auto-context features a_i that are computed from predictions of the previous classifier $P^{t-1}(\cdot|I)$ only. For every pixel i we compute the following auto-context features of length $14C + 1$, where C is the number of classes.

Class probability: The probability $P^{t-1}(c_i|I)$. (length C).

Entropy: The entropy of $P^{t-1}(\cdot|I)$. This feature quantifies the ambiguity of the $t - 1$ stage prediction (length 1).

Row and column scores: We compute the percentage of predicted classes in the row and column of pixel i. Along with this percentage, we compute the average score of all pixels in the same row and column as i (length $4C$).

Distance to the nearest class: Both Euclidean and Manhattan distances to the nearest class pixel are computed as features

(length $2C$).

Class color model: For every class c we fit, with maximum likelihood, a Gaussian distribution to the RGB values of all pixels that are being predicted to be of class c. To be more robust, we fit the distribution only to pixels with probabilities greater than the $3rd$ quartile. For every pixel, we then calculate the log-likelihood for all classes (length C).

Bounding box features: For every class, we fit a rectangular bounding box to every connected component of MAP predictions. For every pixel we compute a C dimensional vector with the c'th component being a 1 or 0 depending on whether it lies inside or outside of a box for class c. A variant of this feature is to compute the average class probability inside the box. This feature aims to improve the segmentation of rectangular objects such as doors and windows (length $2C$).

Neighborhood statistics: For every pixel, the average class probability is computed in a 10×5 region above and below the pixel; and also in a 5×10 region left and right to that pixel (length $4C$).

In the case of point clouds, we use only the class probabilities and the entropy of the class probabilities as auto-context features. So, for point clouds the size of the auto-context features is $C + 1$.

3.5 Stacked Generalization

We train the sequence of classifiers using stacked generalization [7]. The training data is split in M folds and at each stage, M different models are trained using data from $M - 1$ folds, with one fold held out. The M models are used to obtain prediction on the held out fold, this results in a set of cross-validation predictions. It is from these predictions that the auto-context features for training are computed. The next stage classifier is trained subsequently, in the same manner. For every stage, one additional classifier is trained using the entire training data (all M folds) that is used during test-time inference. In our experiments, to segment 2D images we divide the training set into four folds ($M = 4$) and for 3D point clouds, we do not use the stacked generalization ($M = 1$) due to the availability of fewer training points. We use three classification stages for 2D images and only two classification stages for 3D point clouds, as we observe that the performance levels out after that.

Thus, instead of using single classifier in each stage, the auto-context features are computed using predictions from different classifiers, different also from the classifier that will be used at test time. The reason for this procedure is to obtain features that are not computed on training predictions and thus avoid to overfit to the data. This procedure is a standard strategy and is found to be stable and well performing in many scenarios, e.g. [29].

For training and testing, we used the DARWIN toolbox [23]. The maximum tree-depth of each boosted decision tree classifier is set to two and we used a maximum of 200 boosting rounds.

4 EXPERIMENTS

We evaluate the auto-context pipeline on all seven benchmark datasets that are available for the problem of facade segmentation. For all datasets except LabelMeFacade [30] and RueMonge2014 [14] datasets, we report five fold cross-validation results, the standard protocol used in the literature. One fold cross-validation is done for LabelMeFacade and RueMonge2014

datasets as the train and test data splits are pre-specified for these datasets. We compare against all recent best performing methods.

As performance measures, we use the overall pixel-wise classification accuracy, the accuracy averaged over the classes and the intersection over union (IoU) score, popularized by the VOC segmentation challenges [31]. The IoU score is a higher-order loss function and Bayes optimal prediction requires dedicated inference techniques. For simplicity, we report MAP predictions for all pixels and evaluate all three measures on this prediction as done in the literature concerning these datasets. The three measures are defined as follows in terms of false positives (FP), true positives (TP), and false negatives (FN).

- *Overall Pixel Accuracy*: "TP / (TP + FN)" computed over entire image pixels of all classes.
- *Average Class Accuracy*: Pixel accuracy computed for all classes separately and then averaged.
- *Intersection Over Union Score* (IoU): "TP / (TP + FN + FP)" computed on every class and then averaged.

The performance differences are tested for statistical significance. We used a paired t-test with one tail and $p < 0.01$.

4.1 Datasets

ECP Dataset. The ECP dataset [8] consists of 104 rectified facade images of Hausmannian architectural buildings from Paris. For five-fold cross validation, we randomly divide the training data into 4 sets of 20 images and 1 set of 24 images as in [9]. There are seven semantic classes in this dataset.

Graz Dataset. This dataset [3] has 50 facade images of various architectures (Classicism, Biedermeier, Historicism, Art Nouveau) from buildings in Graz. There are only four semantic classes, and the data is divided into 5 equal sets for cross-validation.

eTRIMS Dataset. The eTRIMS dataset [32] consists of 60 non-rectified images. Facades in this dataset are more irregular and follow only weak architectural principles. Again, we split the data into 5 equal sets for cross-validation.

CMP Dataset. This dataset, proposed in [2], has 378 rectified facades of diverse styles and 12 semantic classes in its base set. We divided the data into 4 sets of 75 images each and one set of 78 images for cross-validation.

LabelMeFacade Dataset. Introduced in [30], this dataset has 100 training and 845 testing facade images taken from LabelMe segmentation dataset [33]. Facades in this dataset are highly irregular with a lot of diversity across images.

ENPC Art-deco dataset. This dataset, first used in [34], contains 79 rectified and cropped facade images of the Art-deco style buildings from Paris. Similar to the ECP dataset, the images in this dataset are segmented into seven semantic classes.

RueMonge2014 Dataset. This dataset, introduced in [14], is aimed towards providing a benchmark for 2D and 3D facade segmentation, and inverse procedural modeling. It consists of 428 high-resolution and multi-view images of facades following the Haussmanian style architecture, a reconstructed point cloud, a reconstructed mesh and a framework to evaluate segmentation results. Three tasks are proposed on this dataset in [14, 15] [1]. The first task is the standard image labeling task where each pixel has to be assigned a semantic label. The second task is the mesh labeling task where a semantic label has to be assigned to each face of a given mesh. And the third task is the point cloud labeling

---

1. http://varcity.eu/3dchallenge/

	Door	Shop	Balcony	Window	Wall	Sky	Roof	Average	Overall	IoU
[9]	60	86	71	69	**93**	97	73	78.4	85.1	-
[13]	58	97	81	76	90	94	87	83.4	88.1	-
[10]	79	94	91	85	90	97	90	89.4	90.8	-
[12]	79	**97**	91	**87**	90	97	91	90.3	**91.3**	-
ST1	76	88	86	77	92	97	87	86.0	88.9	75.3
ST2	79	90	89	81	92	**98**	88	88.3	90.5	78.6
ST3	80	92	89	82	92	**98**	88	88.8	90.8	79.3
PW1	78	91	86	77	**93**	**98**	88	87.3	90.0	77.6
PW2	80	92	89	81	**93**	**98**	89	88.9	91.1	79.9
PW3	81	93	89	82	**93**	**98**	89	89.5	**91.4**	**80.5**
Parsing [4]	47	88	58	62	82	95	66	71.1	74.7	-
[5]	50	81	49	66	80	91	71	69.7	74.8	-
ST3+ [4]	64	90	71	76	93	96	77	81.0	**85.2**	72.4

Fig. 3. Segmentation results of various methods on ECP dataset. ST1, ST2, and ST3 correspond to the classification stages in our auto-context method. PW1, PW2, and PW3 refer to a Potts CRF model over the classification unaries. Published results are also shown for comparisons. The parsing results of the reinforcement learning method [4] when using the output ST3 result are reported in the last row.

task where a semantic label has to be assigned to each point in the point cloud. For each of the tasks, fixed splits in training and testing sets are pre-defined. The ground-truth labeling consists of seven semantic classes, same as in the ECP dataset.

4.2 Results on Single-view Segmentation

The empirical results on different datasets are summarized in Fig. 3 for the prominent ECP dataset and in Fig. 4 for the remaining datasets, where ST1, ST2, and ST3 correspond to the classification stages in the auto-context method. In addition to the pixel-wise predictions of the auto-context classifiers, we evaluated a CRF with an 8-connected neighbourhood and pairwise Potts potentials. The single parameter of the Potts model (weight for all classes set to equal) was optimized to yield the highest accuracy on the training set (thus possibly at the expense of losing a bit of performance compared to a cross-validation estimate). Inference is done using alpha expansion implemented in DARWIN [23]. The results of the Potts-CRF on top of the unary predictions of different staged auto-context classifiers are referred to as PW1, PW2, and PW3.

The first observation we make is that the use of a stacked auto-context pipeline improves the results on *all* the datasets. On the ECP dataset, the improvement is 1.9% in terms of overall pixel accuracy for a three-stage classifier (ST3) compared to single-stage classifier (ST1). The ordering in terms of statistically significant performance is ST3>ST2>ST1 on the ECP, CMP, Art-deco and LabelMeFacade datasets and ST3=ST2>ST1 on eTrims and Graz datasets. The auto-context features are frequently selected from the boosted decision trees. For the ECP dataset, about 30% of the features in stage 2 and 3 are auto-context features (CMP 46%, eTrims 31%, and Graz 11%). We didn't notice any significant differences or trends regarding the type of auto-context features picked by the boosted decision trees for different datasets.

The next observation on the ECP dataset is that the overall accuracy of ST3, with 90.8%, is comparable with the reported 91.3% from the current best performing method [12]. The CRF-Potts model (PW3) achieves higher accuracies than the method of [12], making it the (although only marginally) highest published

	[9]	[10]	[19]	[12]	ST1	ST2	ST3	PW3
Average	65.3	65.9	66.4	66.0	74.0	76.8	76.7	**78.1**
Overall	83.2	83.8	83.4	83.5	84.7	86.0	86.1	**87.3**
IoU	-	-	-	-	58.7	61.3	61.5	**63.5**

(a) eTRIMS dataset

	[2]	ST1	ST2	ST3	PW3
Average	47.5	40.5	47.0	**48.7**	**48.9**
Overall	60.3	61.8	65.5	66.2	**68.1**
IoU	-	29.3	34.5	35.9	**37.5**

(b) CMP dataset

	[3]	[12]	ST1	ST2	ST3	PW3
Average	69	**83.5**	79.5	82.4	82.4	**82.6**
Overall	78	**92.5**	90.2	91.1	91.2	**91.7**
IoU	58	-	71.3	73.3	73.3	**74.4**

(c) Graz dataset

	[18]	[35]	ST1	ST2	ST3	PW3
Average	**56.6**	-	47.3	49.2	49.8	49.0
Overall	67.3	71.3	71.5	72.9	73.5	**75.2**
IoU	-	36.0	37.0	38.7	39.4	**39.6**

(d) LabelMeFacades dataset

	[34]	[12]	ST1	ST2	ST3	PW3
Average	72.9	83.8	80.8	84.0	84.3	**84.8**
Overall	78.0	88.8	85.9	88.1	88.3	**89.0**
IoU	58.0	-	68.3	72.0	72.4	**73.5**

(e) Art-deco dataset

Fig. 4. Segmentation results on various 2D datasets. ST1, ST2, and ST3 correspond to the classification stages in the auto-context method. And PW3 refer to a Potts CRF model over ST3 as unaries.

result on the ECP dataset. The results of the auto-context classifier are significantly higher on the other datasets, except in the Graz dataset, when compared to the methods of [3, 10, 9, 2, 18, 35, 19, 12]. On the eTRIMS, CMP and LabelMeFacades datasets, even the first stage classifier produces better predictions than the previous approaches. The methods of [3, 10, 9, 2, 12] all include domain knowledge in their design. For example, the system of [10] is a sequence of dynamic programs that include specific domain knowledge such as that balconies are below windows, that only one door exists, or that elements like windows are rectangular segments. [12] uses hand-written adjacency patterns to limit the possible transitions between different states based on the semantic classes. On the ECP dataset, the authors of [10] and [12] observe respectively, an improvement of about 4% (personal communication) and 1.3% over their unary classifiers accuracy; we conjecture they also may improve the predictions of ST3.

The methods of [3, 10, 9, 2, 18, 35] use different unary predictions and therefore may profit from the output of the auto-context classifier. Unfortunately, the respective unary-only results are not reported, so at this point it is not possible to estimate the relative improvement gains of the methods. The fact that a conceptually simple auto-context pipeline outperforms, or equals, all methods on all published datasets suggests that a more careful evaluation of the relative improvements of [3, 10, 9, 2, 18] is required.

On all the datasets, we observe that the Potts model is improving over the results from the auto-context stages ST1, ST2, and ST3 ($p < 0.01$). This suggests that some local statistics are
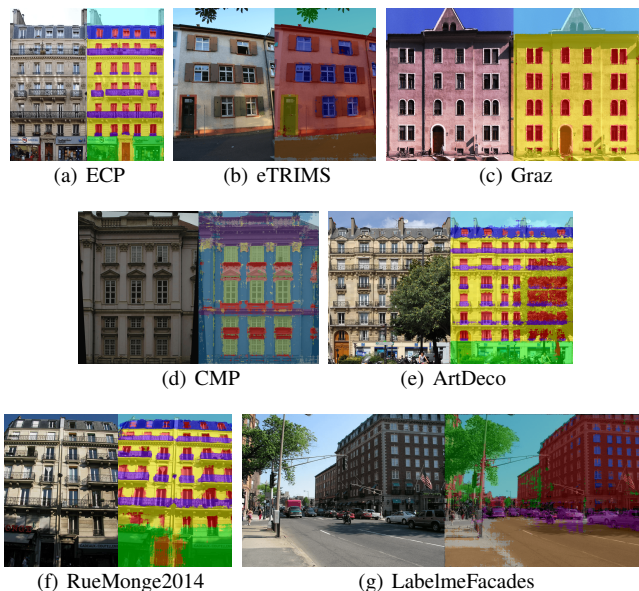
(a) ECP   (b) eTRIMS   (c) Graz

(d) CMP   (e) ArtDeco

(f) RueMonge2014   (g) LabelmeFacades

Fig. 5. Sample segmentation visual results on different 2D facade datasets (best viewed in color and more in supplementary).

Method	Features	AC-Features	ST1	ST2	ST3	PW	[9]	[10]	[12]
Time (s)	3.0	0.6	+0.04	+0.64	+0.64	+24	+110	+2.8	+30

Fig. 6. Average runtime for various methods on a single image of the ECP dataset. 'Features' correspond to low-level and object detection image features (computed once). 'AC-Features' corresponds to Auto-Context features. The classifier runs at 0.04 seconds, every stage needs to additionally compute AC features. A Potts model using alpha expansion takes on average 24s. Inference times (excluding unary computation) of existing methods are also shown for comparison.

not captured in the auto-context features; more local features may improve the auto-context classifiers. In practice, this performance gain has to be traded-off against the inference time of alpha-expansion which is on average an additional 24 seconds for an image from the ECP dataset. Some example visual results (ST3) are shown in Fig. 5 for different datasets and in Fig. 10 for different classification stages. All the results for comparison purpose are publicly available at http://fs.vjresearch.com.

The average runtime of the system on 2D images is summarized in Fig. 6. These numbers are computed on an Intel Core(TM) i7-4770 CPU @ 3.40 GHz for a common image from the ECP dataset (about 500×400 pixels). All the extracted features are computed sequentially one after the other. Fig. 6 also indicates that the proposed approach has favourable runtime in comparison to existing prominent methods.

4.3 Results on Multi-view Segmentation

In this section, we present semantic segmentation results of multi-view scenes using 2D images and 3D point clouds from the RueMonge2014 dataset [14]. The dataset details are already presented in Sec. 4.1. Similar to [15], we show results using only 2D images, only the 3D point cloud and combined 2D+3D data for the tasks of image labeling and point cloud labeling. Additionally, we present results for the mesh labeling task by projecting the image segmentation results and point cloud segmentation results on to the mesh faces.

Here, we first apply the proposed auto-context technique, separately on 2D images and 3D point cloud to measure the relative gains. We find improvements in both 2D and 3D, similar to the results on the single view datasets. For 2D images, the performance levels out after three stages, while for 3D point clouds, the performance levels out after two stages. This can be due to fewer auto-context features and less training data for 3D point clouds. The publicly available 3D point cloud in the RueMonge2014 dataset has only 290196 training points and 276529 test points.

Next, we compare our results with the best performing techniques on these tasks. All the results are summarized in Fig. 7. For all our experiments in 2D, we used the specified training set of 119 images along with ground truth, and evaluated on 202 test images. For the image labeling task, using only 2D images, we perform better (by +2.9% IoU) and faster (by at least a factor of 3) compared to [9]. Note that our runtimes shown in Fig. 7 are computed by applying the proposed technique sequentially on all the 202 test images. This can be easily parallelized by performing the segmentation on all the test images in parallel. Similar improvements in performance are observed in the image labelling task when using only 3D point cloud data as well. Here, the image labeling is performed by back-projecting the semantically-labeled 3D point cloud onto 2D images.

For the point cloud labeling task, using either only 2D or 3D data, we observe better segmentation results compared to [15]. We note that all improvements are obtained without explicitly modeling structural priors or any other type of domain knowledge. [15] proposed to use weak architectural principles in 3D on top of initial segmentations that come from a simple classifier. Such weak architectural principles have shown only a marginal improvement of +0.15% in IoU. In contrast, when using only 3D data, the ST2 result of the proposed auto-context technique performs better by +1.5% in IoU, and improves even further by applying a pairwise Potts model. Note that, in this case, we use exactly the same 3D features as [15] for the first stage classification. This renders the results of weak architectural principles in [15] and the proposed auto-context features directly comparable. We also obtain favorable runtimes. It takes 8 minutes to enforce the weak achitectural principles but less than a minute to apply another stage of auto-context.

	[14]	2D				2D+3D		
		ST1	ST2	ST3	PW3	ST3	ST4	PW4
Average	-	71.6	72.5	72.2	72.2	73.2	79.9	**80.0**
Overall	-	81.7	82.3	82.5	82.8	84.4	84.1	**84.4**
IoU	41.9	57.8	59.0	58.7	58.8	60.9	63.2	**63.7**
Runtime (min)	15	31	60	89	121	89	118	150

Fig. 8. Results for mesh labeling task on the RueMonge2014 dataset.

Next, similar to [15], we combine the segmentation results of 2D images and 3D point clouds for further improving the performance ('2D+3D' in Fig. 7). For this, we accumulate the ST3 and ST2 results of 2D images and 3D point cloud respectively. Further applying auto-context (ST4) on the accumulated unaries boosts the IoU performance by another 2.1% in labeling the point cloud, while it levels out in labeling the images. Additionally, applying a pairwise Potts CRF model similar to [15] to enforce smoothness, further increases the IoU performance by 0.7% and 0.2% in labeling the images and point cloud respectively. In

	2D					3D					2D+3D					
	[9]	ST1	ST2	ST3	PW3	**[14]**	**[15]**-3	ST1	ST2	PW2	**[15]**-5	**[15]**-7	ST3	ST4	PW3	PW4
Average	-	72.6	72.8	72.7	73.7	-	-	68.0	67.8	68.3	-	-	74.2	77.9	74.4	**79.0**
Overall	-	79.1	79.4	80.0	81.2	-	-	78.2	82.0	82.3	-	-	**82.7**	80.9	83.4	81.9
IoU	57.5	58.1	58.4	58.9	60.5	41.3	53.2	54.3	56.3	57.0	61.3	62.0	62.0	61.2	**62.7**	62.7
Runtime (min)	379	27	56	85	117	15	21	19	19	20	324	404	85	114	117	146

(a) Image labeling

	2D							3D						2D+3D				
	[9]	**[15]**-1	**[15]**-2	ST1	ST2	ST3	PW3	**[14]**	**[15]**-3	**[15]**-4	ST1	ST2	PW2	**[15]**-5	**[15]**-6	ST3	ST4	PW4
Average	-	-	-	70.8	71.9	72.6	72.7	-	-	-	63.7	68.0	68.5	-	-	73.3	**75.4**	75.3
Overall	-	-	-	79.3	80.9	81.6	82.1	-	-	-	78.8	77.9	78.6	-	-	84.3	84.4	**84.7**
IoU	56.1	55.7	55.4	55.7	57.1	58.2	58.6	42.3	52.1	52.2	51.3	53.6	54.4	60.1	60.8	60.6	62.7	**62.9**
Runtime (min)	382	302	380	28	57	86	118	15	15	23	15	15	16	317	325	86	86	87

(b) Point Cloud labeling

Fig. 7. Segmentation results of various methods for the tasks of (a) image labeling and (b) point cloud labeling on the RueMonge2014 dataset. In the following, L1 and L2 represent the first and second layers of [9]. RF refers to the random forest classifier in [15]. 3DCRF refers to a Potts model-based CRF defined on 4-nearest neighbourhood of the point cloud. 3DWR refers to weak architectural principles from [15]. The headings are defined as [15]-1 = L1+3DCRF, [15]-2 = L1+3DCRF+3DWR, [15]-3 = RF+3DCRF, [15]-4 = RF+3DCRF+3DWR, [15]-5 = RF+L1+3DCRF, [15]-6 = RF+L1+3DCRF+3DWR, and [15]-7 = RF+L2. The runtimes shown here, in minutes, include the feature extraction, classification and optional projection on the entire dataset. Note that, in case of 2D, the specified runtimes are the time taken to segment all 202 test images sequentially.

summary, as evident in Fig. 7, better performance than existing state-of-the-art approaches is obtained in both image and 3D point cloud labeling, while being 2-3 times faster. A visual result of 3D point cloud segmentation is shown in Fig. 9

Finally, we compare our results with existing approaches on the mesh labeling problem. To label meshes, the 2D image segmentation results are projected onto the mesh faces. 2D segmentation results obtained with only 2D images and with both 2D+3D data are used for mesh labeling. See Fig. 8 for quantitative results and Fig. 9 for a visual result. Again we observe similar improvements with auto-context classifiers. Our simple majority voting scheme to project the semantics from 2D images to 3D mesh shows that we perform significantly better (by +17.4% IoU) in comparison to the existing approach from [14]. However this comes at a cost of runtime (6 × slower). The result of earlier stages of our auto-context technique still performs better, 'ST1' for example, by +15.9% with a comparable runtime. In [14], 3D information is used to reduce redundant evaluations, thereby achieving faster runtime.

4.4 Inverse Procedural Modeling

A pixel-wise classification of a facade might not be the desired input for some applications. This fact motivated shape grammar methods [3, 36, 4, 5] that parse the facade into a high-level structured representation. The aim of these top-down approaches is to infer the architectural (structural) information in facades by fitting a set of grammar rules (a derivation) to a pixel classifier output. Such structural information can be used for retrieving structurally similar facades, etc. We apply the parsing method of [4] and compare against their result, that is obtained using a random forest classifier that uses color information. All other settings and the grammar are the same. We refer the reader to [4] for more details about the approach. The results are shown in the last three rows of Fig. 3. These numbers are obtained by back-projecting the parsed representation into a pixel-wise prediction. We observe that better pixel predictions directly translates to better parsing results. A substantial improvement of 10.5% is achieved, closing the gap to pixel prediction methods. This shows the importance of good pixel predictions even for models that only

make use of them as an intermediate step. Fig. 10 shows a sample visual result of various classification stages and the parsing result obtained with ST3 + [4].

5 CONCLUSION

The segmentation method that we described in this paper is a framework of established and proven components. It is easy to implement, fast at test-time, and it outperforms all previous approaches on all published facade segmentation datasets. It is also the fastest method amongst all those that we compared against. The runtime is dominated by feature computation, which is amenable to massive speed improvements using parallelization in case a high-performing implementation is required.

We observe on all datasets that adding stacked classifiers using auto-context features improves the performance. This applies to both 2D (images) and 3D (point clouds) data. For the ECP dataset, a Potts-CRF further improves the performance but this comes at the expense of a severe increase in runtime. Further, the proposed technique can be applied independently to either 2D or 3D data and also to combined 2D+3D models. For the point cloud labeling task, on RueMonge2014 dataset, applying auto-context on the combined 2D+3D improves the IoU performance by 1.9%.

The proposed auto-context classifier raises the bar when it comes to absolute performance. Contrary to the popular belief in this domain, it largely ignores domain knowledge, but still performs better than all the methods that include prior information in some form, for example relationship between balconies and windows. We believe that it is important to evaluate methods in terms of a relative improvement over strong pixel classifier baselines. In order to facilitate a fair comparison of previous and future work, we release all code that has been used to obtain the reported results along with all predictions for easy comparison[2].

2. http://fs.vjresearch.com

| (a) Point Cloud | (b) Ground Truth | (c) ST4 |

| (a) Mesh Surface | (b) Ground Truth | (c) ST4 |

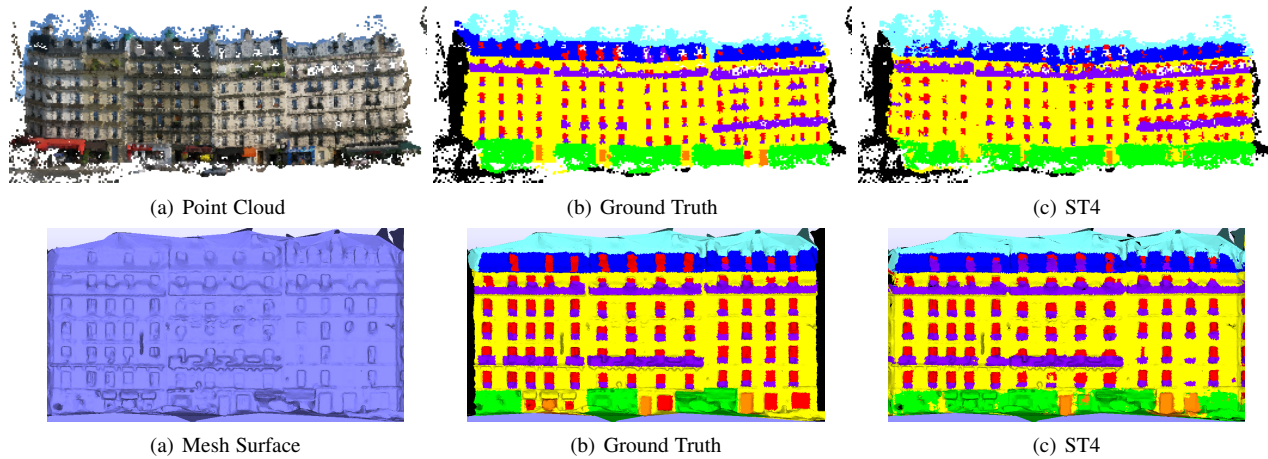Fig. 9. Sample visual results for the point cloud and mesh labeling tasks on the RueMonge2014 dataset (More in supplementary).

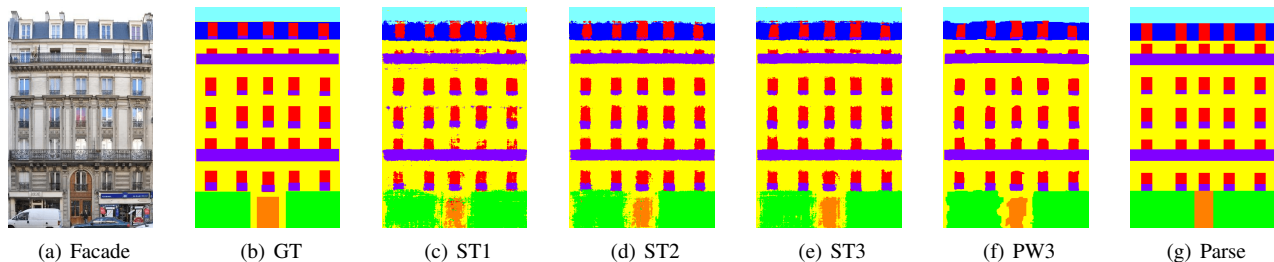| (a) Facade | (b) GT | (c) ST1 | (d) ST2 | (e) ST3 | (f) PW3 | (g) Parse |

Fig. 10. (a) Sample facade image from ECP dataset; (b) Ground truth segmentation; and (c,d,e) Result of various classification stages of our auto-context method. Observe that the method removes isolated predictions and recovers the second lowest line of windows. (f) Potts model on top of ST3 result, and (g) parsed result obtained by applying reinforcement learning [4] using ST3 result.

REFERENCES

[1] M. Y. Yang and W. Forstner, "A hierarchical conditional random field model for labeling and classifying images of man-made scenes," in *ICCV Workshops*, 2011.

[2] R. Tylecek and R. Sara, "Spatial pattern templates for recognition of objects with regular structure," in *GCPR*, 2013.

[3] H. Riemenschneider, U. Krispel, W. Thaller, M. Donoser, S. Havemann, D. Fellner, and H. Bischof, "Irregular lattices for complex shape grammar facade parsing," in *CVPR*, 2012.

[4] O. Teboul, I. Kokkinos, L. Simon, P. Koutsourakis, and N. Paragios, "Shape grammar parsing via reinforcement learning," in *CVPR*, 2011.

[5] A. Martinovic and L. Van Gool, "Bayesian grammar learning for inverse procedural modeling," in *CVPR*, 2013.

[6] Z. Tu, "Auto-context and its application to high-level vision tasks," in *CVPR*, 2008.

[7] D. H. Wolpert, "Stacked generalization," *Neural Networks*, 1992.

[8] O. Teboul, "Ecole centrale paris facades database," 2010.

[9] A. Martinovic, M. Mathias, J. Weissenberg, and L. Van Gool, "A three-layered approach to facade parsing," in *ECCV*, 2012.

[10] A. Cohen, A. G. Schwing, and M. Pollefeys, "Efficient structured parsing of facades using dynamic programming," in *CVPR*, 2014.

[11] M. Koziński, G. Obozinski, and R. Marlet, "Beyond procedural facade parsing: Bidirectional alignment via linear programming," in *ACCV*, 2014.

[12] M. Kozinski, R. Gadde, S. Zagoruyko, R. Marlet, and G. Obozinski, "A MRF shape prior for facade parsing with occlusions," in *CVPR*, 2015.

[13] M. Mathias, A. Martinović, and L. Van Gool, "ATLAS: A three-layered approach to facade parsing," *IJCV*, 2015.

[14] H. Riemenschneider, A. Bódis-Szomorú, J. Weissenberg, and L. Van Gool, "Learning where to classify in multi-view semantic segmentation," in *ECCV*, 2014.

[15] A. Martinovic, J. Knopp, H. Riemenschneider, and L. Van Gool, "3d all the way: Semantic segmentation of urban scenes from start to end in 3d," in *CVPR*, 2015.

[16] L. Ladickỳ, P. Sturgess, K. Alahari, C. Russell, and P. H. Torr, "What, where and how many? combining object detectors and crfs," in *ECCV*, 2010.

[17] J. Tighe and S. Lazebnik, "Superparsing: scalable nonparametric image parsing with superpixels," in *ECCV*, 2010.

[18] B. Fröhlich, E. Rodner, and J. Denzler, "Semantic segmentation with millions of features: Integrating multiple cues in a combined random forest approach," in *ACCV*, 2012.

[19] C. Gatta and F. Ciompi, "Stacked sequential scale-space taylor context," *PAMI*, 2014.

[20] J. Shotton, J. Winn, C. Rother, and A. Criminisi, "Textonboost: Joint appearance, shape and context modeling for multi-class object recognition and segmentation," in *ECCV*, 2006.

[21] N. Dalal and B. Triggs, "Histograms of oriented gradients for human detection," in *CVPR*, 2005.

[22] T. Ojala, M. Pietikäinen, and T. Mäenpää, "Multiresolution gray-scale and rotation invariant texture classification with local binary patterns," *PAMI*, 2002.

[23] S. Gould, "DARWIN: A framework for machine learning and computer vision research and development," *JMLR*, 2012.

[24] D. Ok, M. Kozinski, R. Marlet, and N. Paragios, "High-level bottom-up cues for top-down parsing of facade images," in *3DIMPVT*, 2012.

[25] M. Kozinski and R. Marlet, "Image parsing with graph grammars and markov random fields," in *WACV*, 2014.

[26] P. Dollár, Z. Tu, P. Perona, and S. Belongie, "Integral channel features." in *BMVC*, 2009.

[27] P. Dollár, "Piotr's Computer Vision Matlab Toolbox (PMT)," http://vision.ucsd.edu/~pdollar/toolbox/doc/index.html, 2014.

[28] A. E. Johnson and M. Hebert, "Using spin images for efficient object recognition in cluttered 3d scenes," *PAMI*, 1999.

[29] P. Gehler and S. Nowozin, "On feature combination for multiclass object classification," in *ICCV*, 2009.

[30] B. Frohlich, E. Rodner, and J. Denzler, "A fast approach for pixelwise labeling of facade images," in *ICPR*, 2010.

[31] M. Everingham, L. Van Gool, C. K. Williams, J. Winn, and A. Zisserman, "The pascal visual object classes (voc) challenge," *IJCV*, 2010.

[32] F. Korc and W. Forstner, "eTRIMS Image Database for interpreting images of man-made scenes," Dept. of Photogrammetry, University of Bonn, Tech. Rep. TR-IGG-P-2009-01, April 2009.

[33] B. C. Russell, A. Torralba, K. P. Murphy, and W. T. Freeman, "Labelme: a database and web-based tool for image annotation," *IJCV*, 2008.

[34] R. Gadde, R. Marlet, and N. Paragios, "Learning grammars for architecture-specific facade parsing," *IJCV*, 2016.

[35] S. Nowozin, "Optimal decisions from probabilistic models: the intersection-over-union case," in *CVPR*, 2014.

[36] N. Ripperda and C. Brenner, "Reconstruction of façade structures using a formal grammar and RjMCMC," in *DAGM*, 2006.